Supplementary Methods

Animal care:

Six wild-caught snipefish (*Macroramphosus scolopax*) were housed individually in 100 liter aquaria in a temperature-controlled room maintained at 17°C. Fish were filmed while feeding on larval zebrafish in their housing tank with a Fastec HiSpec 1 system (San Diego, CA, USA) at 2000 frames/s. Two 120 W halogen lights were used to light the field of view during filming. Distances in the video images were calibrated with a ruler placed in the tank at the location of the feeding strikes. At least 10 high quality feeding videos were collected for each individual snipefish based on the following criteria: the fish appeared to be oriented perpendicular to the plane of the camera, the head and most of the body (at least one head-length) were in view, and the prey was successfully captured. We then selected the five strikes for each individual with the shorted time to prey capture (time between onset of hyoid depression and prey capture). After filming, fish were euthanized with an overdose of MS-222, photographed using a Nikon D90 with a 60mm lens, and the muscles powering suction feeding (epaxials, hypaxials, sternohyoideus), were dissected and weighed (wet weight) for use in calculation of power requirement.

Basic feeding kinematics:

We used the MATLAB program DLTdv3 (Hedrick, 2008) to digitize 9 landmarks in each frame of the high-speed videos in our analysis (Supplemental Fig. S1). Landmark tracking began 6 frames prior to hyoid movement (depression) and was continued to at least 5 frames after prey capture (defined as the frame at which the center of mass of the prey passes into the mouth). Point 1 marked the anterior tip of the upper jaw (premaxilla). Point 2 marked the anterior tip of the lower jaw (dentary). Point 3 marked a stationary landmark on the dorsal portion of the body. Because point 3 was used in the calculation of head angle relative to the body, it was placed as far from the back of the head as possible (but anterior to the dorsal spine) to decrease error in the measurement of this focal angle. Point 4 tracked the center of mass of the prey. Point 5 tracked a stationary background point. Point 6 was used to track the hyoid rotation point, or the approximate location of the hyoid-suspensorium joint. From X-rays and micro-CT scans, we were able to verify that this joint is roughly internal to the inflection in the preoperculum (Supplemental Fig. S1). Point 7 marked a stationary point on the head, usually anterior to the eye. Point 8 marked the distal tip of hyoid bar (ceratohyal). This was the only landmark that could not be digitized on every frame, since the hyoid was not visible before the onset of hyoid rotation (depression). To obtain an estimate of the initial hyoid angle, point 8 was placed at a position even with the ventral margin of the head on the frame just prior to hyoid onset (Supplemental Fig. S1A). The hyoid was then tracked normally starting on frame 7, when it was visible. Finally, point 9 tracked the joint between the head and the body (posttemporal-supracleithrum joint).

Gape was measured as the change in the distance between the jaw tips, or the distance between points 1 and 2. Head rotation relative to the body was measured as the change in angle between points 1, 9 and 3. Hyoid rotation was measured as the change in angle between points 7, 6, and 8. The raw values for gape, head rotation, and hyoid rotation were each smoothed using a 5^{th}-order polynomial function prior to downstream

calculations, including calculation of rotational velocities and accelerations. Onset of gape and head rotation was set to the minimum recorded value. Hyoid had a definitive onset since it is initially hidden, so hyoid onset was set to frame 6, or the frame before the hyoid is first visible. Because variables often exhibited asymptotic trends near their peak values with respect to time, time at peak gape, head rotation, and hyoid rotation were each determined as the time at which the variable is at least 95% of its peak value. Total change in gape, head rotation, and hyoid rotation were calculated as the difference between the minimum and maximum recorded values during a sequence. Finally, time to prey capture was calculated as the time between hyoid onset (frame 6) and prey capture (the first frame in which the prey, point 4, passes through the invisible line between the jaws formed by points 1 and 2). The relative displacements and timings for a typical feeding strike are shown in Figure 1.

Calculation of muscle-mass specific power requirement:
To remain consistent with Van Wassenbergh et al. (2008), we digitized a series of 10 landmarks on frames of the high-speed videos to obtain kinematic variables to estimate power (Supplemental Fig. S2A). Digitization began one frame before hyoid movement and continued until prey capture. Because the model calculates the power used for head rotation and recoil of the body separately, it is important that head rotation is calculated relative to the earthbound frame of reference (versus relative to the body). Points 1-4 were used to determine head rotation. 1 and 2 marked the dorsal and ventral margin of the snout and were placed just behind the dentary (to remove the effect of mouth opening). Points 3 and 4 marked dorsal and ventral stationary points on the head. Unlike Van Wassenbergh et al., we did not place these landmarks directly on the dorsal and ventral margins of the head since this is hard to digitize accurately during rotation. A line was then drawn between the midpoint of 1 and 2 and the midpoint of 3 and 4, to find the orientation of the head in each frame. Head rotation (delta theta) was calculated relative to the earthbound frame of references as the change in orientation between this line through the head and the orientation of this line at the start of the video. Head rotation was then smoothed using a zero-phase shift low-pass butterworth filter. We used a 1000 Hz cutoff (0.5 sample frequency) since this appeared to work best for our data and framerate. Angular velocity was calculated from the smoothed delta theta values and then further filtered for noise with a 2 point moving average. The same was repeated for angular acceleration. This results in very conservative estimates of maximum angular velocity and acceleration.

Points 5 and 6 were placed approximately 1 head length posteriorly on the body of the fish. Points 7 and 8 marked the dorsal and ventral margins (respectively) of the body at the back of the head. A line drawn between the midpoint of 5 and 6 and the midpoint of 7 and 8 was used to determine the longitudinal axis of the body at the start of the video, and only needed to be digitized in the first frame. Points 9 and 10, marked the tip of the snout and the back of the operculum and were used to calibrate small differences in cranial length measured in the video to the lengths measured from photos of the corresponding specimen.

Two important parameters that must be specified for the model include the proportion of the body that recoils during the feeding strike and the amount (and identity) of muscles assumed to contribute to powering dorsal head rotation. For snipefish, we set

the proportion of the body (p) to be half of the head length, which matches observations from videos that the body recoils from approximately the back of the head to the insertion of the dorsal spine (about half a head length down the body for all individuals). The identity and amount of muscle used for head rotation in fish is still an active area of research (Camp et al., 2015), and has not been studied in snipefish specifically. We included the entire sternohyoideus muscle and the anterior portion of the hypaxial musculature, which can act together to pull posteriorly on the hyoid apparatus, whose motion is coupled to head rotation by a four bar linkage (described in more detail in the main text). We also included the anterior portion of the epaxial muscles. The epaxials are generally accepted to be the largest contributor to head rotation during suction feeding in fishes by exerting force directly on the back of the neurocranium. In most fishes, it is not obvious what proportion of the epaxial (and hypaxial) muscles are recruited for head rotation. However, in snipefish, removal of the dorsal armor plates revealed epaxial muscles that are morphologically distinct from the posterior epaxial musculature (Supplemental Fig. S2B-C). These anterior muscles on the right and left were separate and housed in the space between the armor and reinforced neural spines (Fig. 3 and Fig. S2). Instead of being composed of obvious myomeres, they appear as cylindrical bundles of fibers, covered with shiny tissue. The dorsal and ventral portions of the epaxials were only loosely connected to one another and divided by a large flexible tendon. The anterior portions of the epaxials are so markedly different from the posterior region of the epaxials, which assume the normal appearance of myomeres, that we see this as convincing grounds to assume that the two portions are specialized for different functions (powering feeding, versus powering locomotion). Although there is no such contrast between the anterior and posterior portions of the hypaxial muscles, we divided them into two parts along the same cut as the epaxials for consistency, while including most of the overlying pectoral musculature to be conservative.

Micro-CT and digital radiography:
Two snipefish specimens similar in size to those used in feeding analyses were euthanized with an overdose of MS-222 and formalin-fixed. One specimen was fixed in the pre-strike position, with the hyoid, suspensorium, and operculum fully adducted. The second specimen was fixed in a posture seen near the end of feeding strikes, with the head elevated and the hyoid rotated past 90 degrees. Pins were used to keep the head elevated during fixing, but were not needed for the adducted specimen. Specimens were allowed to air dry and scanned individually using an Inveon MM CT at a resolution of 35.464µm. Scans were converted to DICOM format and 3D reconstructions and surface renderings were made using Amira and OsiriX MD. Air-drying specimens allowed for visualization of muscles and even some tendons in volume rendering. Digital radiography was carried out at the Smithsonian Museum of Natural History using a Varian 4030 Panel capable of exposures from 40 to 120 KV. Specimens were oriented laterally with respect to the beam. In addition to radiographing the two fixed specimens we described above, we also radiographed an additional individual with the suspensorium and hyoid adducted from the museum's collections (USNM_402455) to verify the arrangement of the four bar linkage. Radiograph images can be found in Figure S6.

Four-bar linkage analysis:

The arrangement of the four-bar linkage was traced onto 2D radiograph images in Adobe, using the micro-CT scans and euthanized specimens as a guide. The connection between the urohyal-sternohyoideus linkage and the pectoral girdle is the only "joint" that is not immediately obvious from osteology. We determined this location on radiographs by passing a straight line directly through the urohyal, beginning at the notch on the ventral surface of the anterior ceratohyal where a ligament connects it to the urohyal and continuing the line through the urohyal until reaching the pectoral girdle. The sternohyoideus bridges the space between the urohyal and pectoral girdle in specimens. Thin extensions of the hypaxial musculature also pass laterally around the pectoral girdle as it tapers towards its connection with the bony armor on the ventral midline, and the muscle from each side inserts ventrally on urohyal. The urohyal-sternohyoidues linkage is reinforced ventrally by a plate of armor.

Using Grashof's criterion and measured linkage lengths, we determined that the snipefish four-bar mechanism must function as a crank-rotator system with the hyoid link (h) as the crank. Since we were interested in head elevation and hyoid depression (the angles between n and p and h and n respectively), we assigned the longest link, the neurocranium-suspensorium link (n) as the stationary link. The hyoid link (h) is the shortest link (the crank) and one of the sides, making the pectoral girdle link, p, the other side. The urohyal-sternohyoideus link (u) functions as the coupler. Although the crank is conventionally assigned as the input link in a linkage analysis, because of the biology of the system, we made p our input link since we expect force from the epaxial and hypaxial muscle to elevate the head (increasing the input angle, theta). The output angle, τ, is therefore the angle between n and h. Making p the input link (versus h) is valid from a biomechanical perspective, since either link adjacent to the stationary link can be considered as the input link.

We used high-resolution micro-CT scans to describe morphological features related to the snipefish feeding mechanism and digital radiographs to measure relative lengths and angles of the proposed four-bar linkage mechanism. We also validated the four-bar linkage mechanism by digitizing the locations of all four rotation points on video sequences and testing to see if we could use the model to make accurate predictions of movement. Specifically, we predicted the output angle (hyoid rotation: angle between h and u) in each frame given the measured input angle (head angle: angle between n and p) and the initial linkage lengths in the frame in each frame of the video. Note that we began digitization for this analysis on the first frame after the hyoid began rotating. Among the four rotation points, only the insertion of the sternohyoideus on the pectoral girdle is not clearly visible. Instead, this joint was inferred based on the orientation of the sternohyoideus musculature in the video and an understanding of the snipefish morphology from studying the micro-CT scans. To test for significance of our measured and predicted angles hyoid angles, we calculated T-statistics between the predicted and measured output angles for each individual in each frame. P-values were adjusted using the Holm-Bonferroni method to correct for multiple comparisons.

Assumptions and caveats:

In snipefish, hypothesize that the anterior epaxial and hypaxial muscles are the "motor," the enlarged epaxial tendons function as the "spring", a torque reversal four-bar linkage forms the "latch," a the sternohyoideus and slips of the hypaxial act as the

"trigger." However, muscle activation patterns are needed to verify these designations. For instance, in snipefish, how much muscle mass contributes to power production during energy storage? Recent research has shown that large amounts of both the epaxial and hypaxial muscles power suction feeding motions in largemouth bass (Camp and Brainerd, 2015), and both sets of muscles are active prior to observed head rotation in seahorses (Van Wassenbergh et al., 2014). The epaxial muscles in snipefish are unusual compared to other fishes because the anterior portion is differentiated from the posterior portion behind the dorsal spine. For this reason, we assumed that the anterior epaxial musculature is specialized for feeding in snipefish. To be conservative, we also included the anterior hypaxial muscles and sternohyoideus muscle in our calculated power requirement. Concerning the latch, it is possible (even probable) that contraction of the adductor arcus palatini (AAP) reinforces the latch in snipefish by adducting the suspensorium and preventing hyoid depression. Activation of the AAP during loading appears to be necessary for achieving extremely high power outputs in seahorses (Van Wassenbergh et al., 2014). However, because the hyoid never became unlatched during manipulation of euthanized snipefish, we do not believe that other muscle activity is necessary to latch the system, although it cannot be ruled out with out direct evidence from approaches like EMG. Likewise, high-speed fluoroscopy or related methods could verify that the over-center four-bar arrangement we show in preserved specimens is true to the arrangement in live snipefish.

References:

Camp, A. L., Roberts, T. J. and Brainerd, E. L. (2015). Swimming muscles power suction feeding in largemouth bass. *Proc. Natl. Acad. Sci.* **2015**, 201508055.

Hedrick, T. L. (2008). Software techniques for two- and three-dimensional kinematic measurements of biological and biomimetic systems. *Bioinspir. Biomim.* **3**, 034001.

Van Wassenbergh, S., Dries, B. and Herrel, A. (2014). New insights into muscle function during pivot feeding in seahorses. *PLoS One* **9**, e109068.

Supplementary Figures and Tables

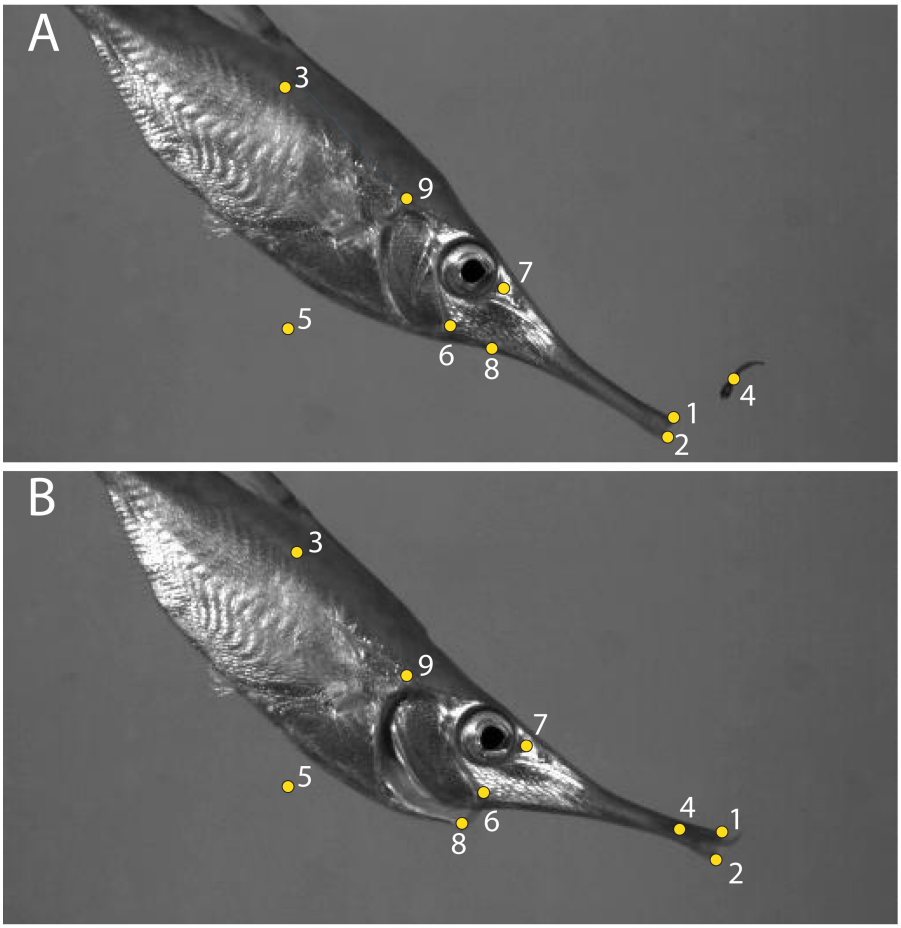

Figure S1: Landmarks digitized for kinematic analysis of snipefish feeding shown on frames from two frames in a typical strike, just before the onset of hyoid rotation (**A**) and after prey capture (**B**). Detailed descriptions of landmark placements and usage in analyses can be found in the text.

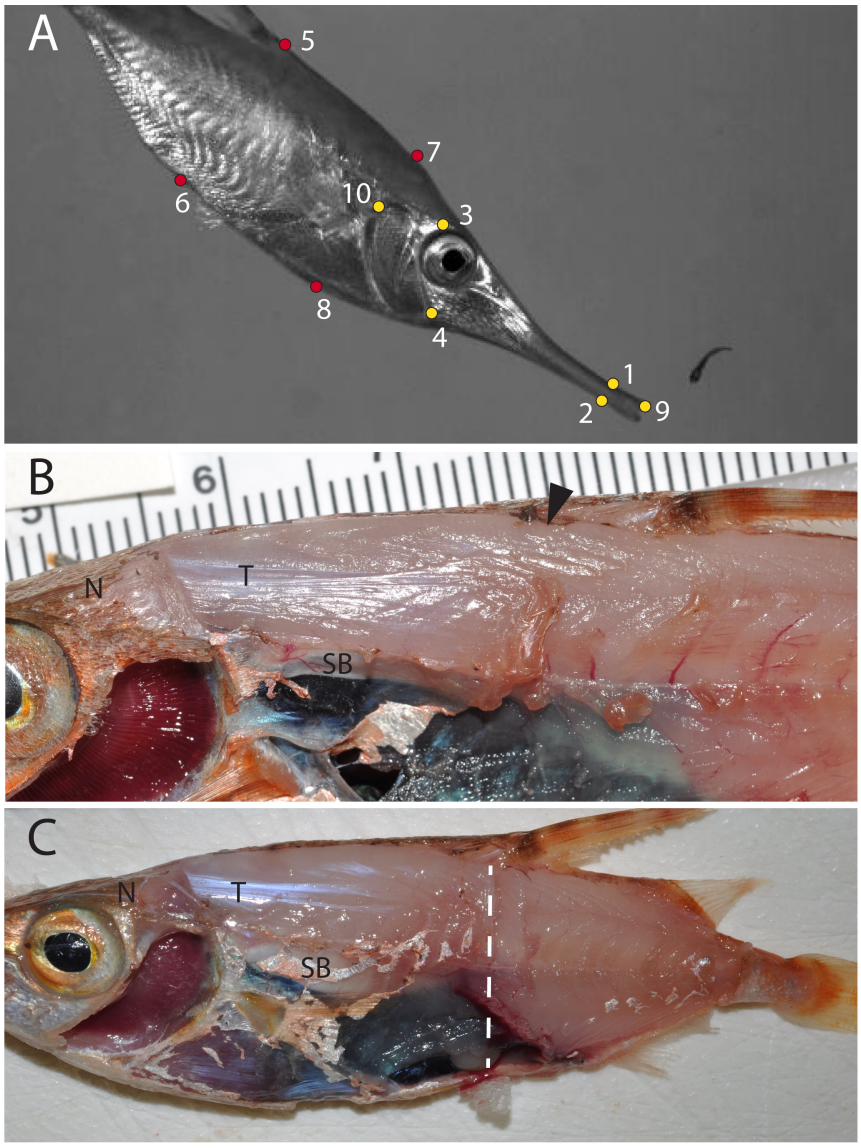

Figure S2: **A**. Landmarks digitized for calculations of the power requirement for head rotation and body recoil during snipefish feeding shown on a frame just before the onset of hyoid rotation. **B**. Dissection showing anterior epaxial muscle. The transition to "normal" myomeres is indicated with an arrow. The large epaxial tendon is easily seen (T). **C**. Location of cut between anterior and posterior hypaxial and epaxial muscles is shown (dotted line).

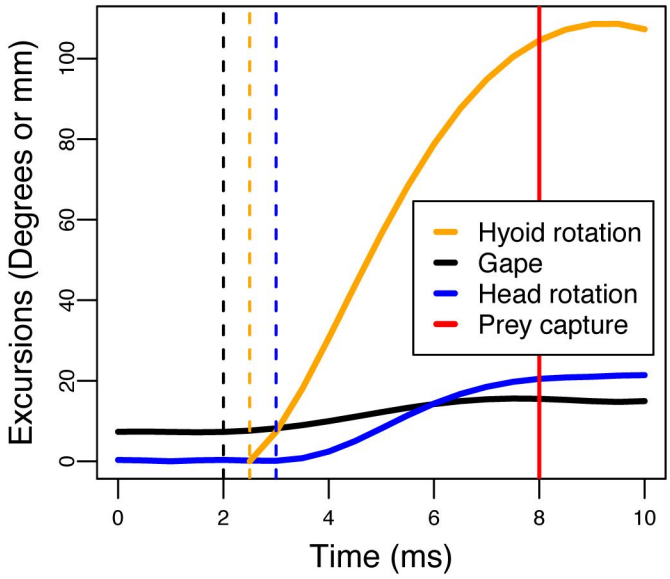

Figure S3: Kinematics of a typical snipefish strike. Dashed lines indicate the onset times of hyoid rotation (orange), mouth opening (black) and head rotation (blue). The red line indicates time of prey capture. Head rotation and hyoid rotation are in units of degrees and gape is measured in millimeters (gape). Figure 1 shows the same kinematics as proportions.

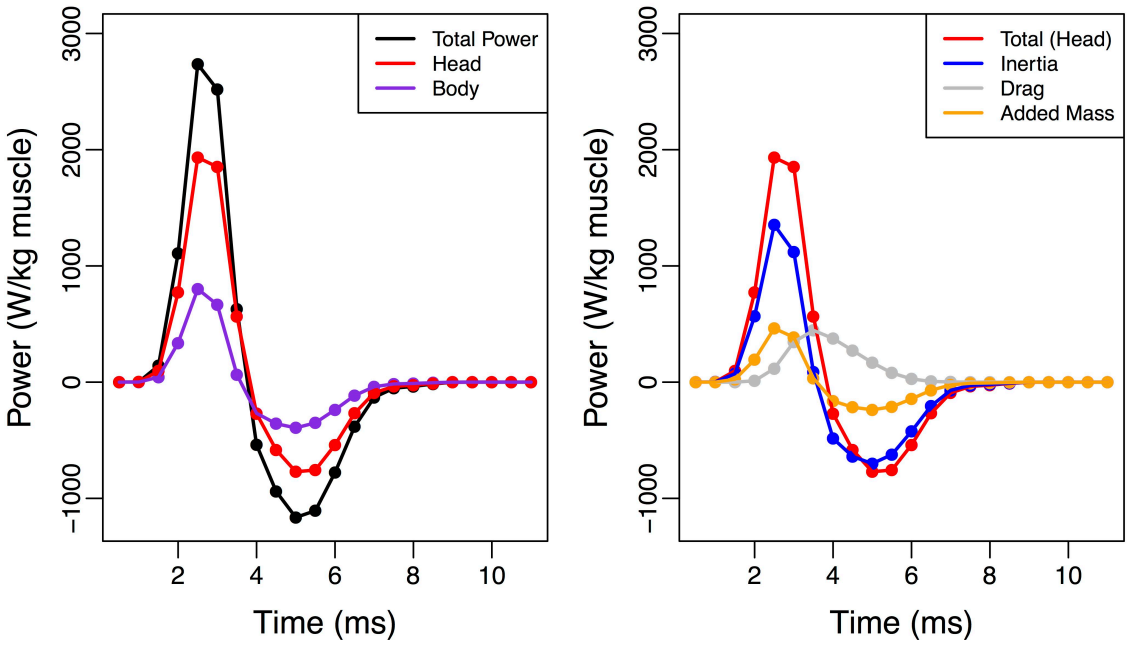

Figure S4: Profiles of muscle mass specific power requirement during a typical snipefish feeding strike. Peak power (left, black) is achieved early (2.5 ms) and the power needed to rotate the head contributes most (red) compared to the body (purple). Focusing on the power requirement just to rotate the head (right), power required to overcome the inertial forces on the head (blue) are greatest at the time of maximum power requirement.

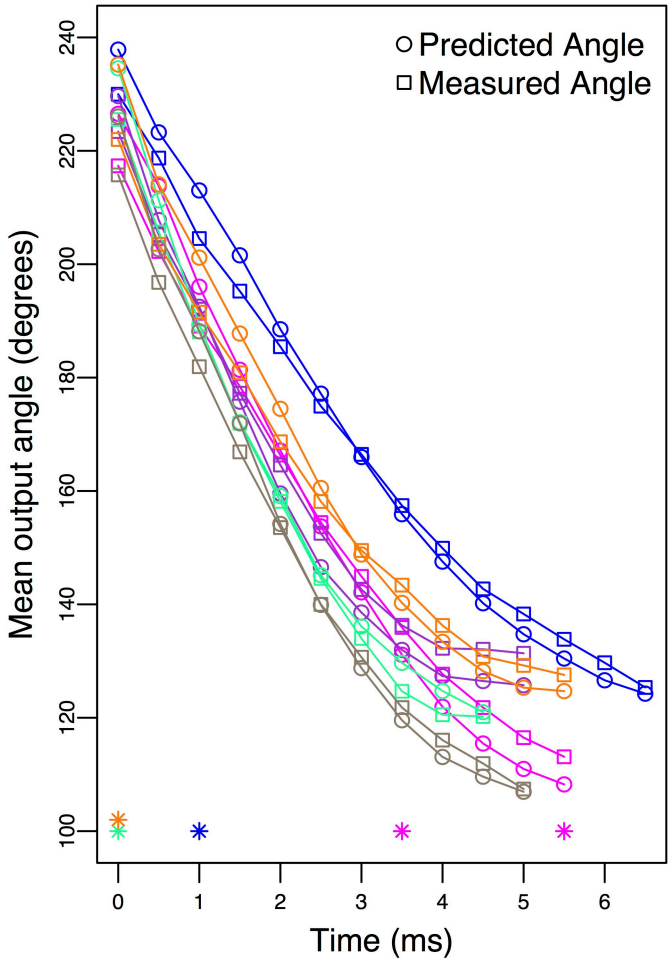

Figure S5: Validation of the four-bar linkage mechanism during feeding strikes. Given head angle in each frame of the video and initial linkage lengths, the output angle ("hyoid angle") is accurately predicted. Different individuals are shown in different colors. Asterisks (*) indicate frames in which the measured and predicted output angle for an individual were significantly different (Holm-Bonferroni corrected p-value <0.05).

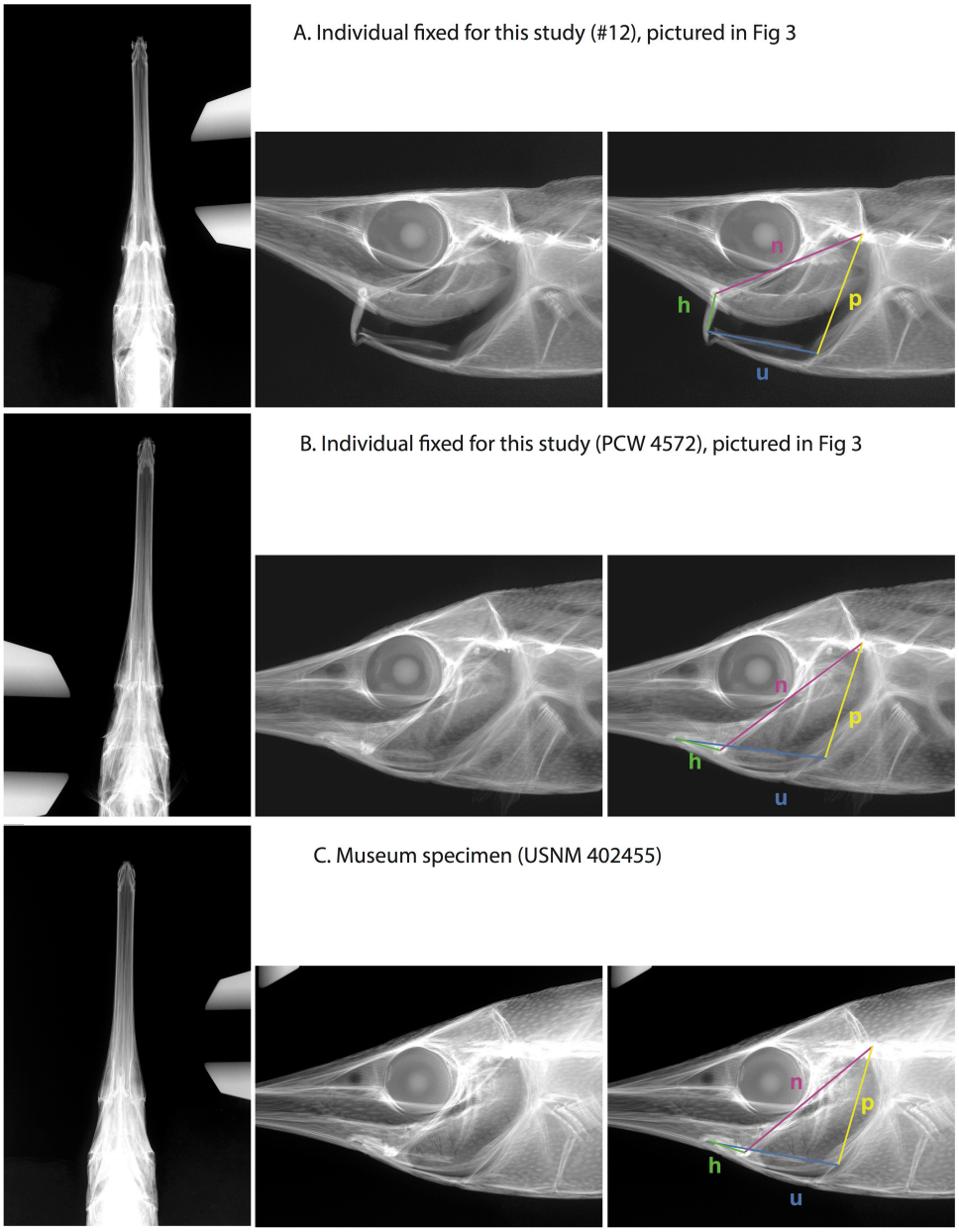

Figure S6: Radiographs from specimens used to evaluate the arrangement of the four-bar linkage mechanism. **A.** Specimen fixed by S. Longo with the hyoid depressed. This specimen was radiographed and micro-CT scanned. **B.** Specimen fixed by S. Longo with the hyoid and suspensorium adducted and the head depressed. This specimen was radiographed and micro-CT scanned. **C.** Specimen from the Smithsonian National Museum of Natural History, which was also radiographed. Each specimen is shown in dorsal view (left), lateral view (middle), and lateral view with the linkage mechanism overlaid (right). Pink= neurocranium-suspensorium linkage (n) . Yellow= pectoral linakge (p). Blue = urohyal-sternohyoideus linkage (u). Green = Hyoid linkage (h). Scale = 1 cm.

Supplementary Tables

Individ.	Time to prey capture (ms)	Relative gape onset (ms)	Relative head rotation onset (ms)	Gape (mm)	Hyoid rotation (deg)	Head rotation (deg)	Hyoid velocity (deg/s)	Head velocity (deg/s)
1	6.8	-0.8	0.7	1.4	119	20.7	24000	4710
2	5.5	-1.7	0.5	1.3	110	22.6	25600	5570
3	4.4	-1.5	0.5	0.8	116	18.6	36000	6800
4	4.6	-1.7	0.2	1.2	109	19.0	35800	6650
5	5.8	-0.4	0.8	1.4	108	18.5	27500	5790
6	4.7	-0.4	0.4	1.8	121	22.5	32500	7020
Mean	5.3	-1.08	0.52	1.3	114	20.3	30200	6090
SD	0.92	0.62	0.21	0.3	5.6	1.9	5300	890
min	2	-2.5	0	0.6	92	15.2	18700	3330
max	7.5	0	1	2.1	133	25.3	47000	8670

Table S1: Snipefish feeding kinematics and peak power requirement. Average kinematic variables were calculated for each of the 6 individual (individ.) fish in our study. We also report the mean and standard (SD) deviation across individuals. Minimum (min) and maximum (max) values are calculated across all 30 strikes to show the range in the entire dataset. The timing of the onsets of gape and head rotation are calculated relative to the onset of hyoid movement, so that negative values indicated onsets before the hyoid begins depressing.

Individ	Peak Power (W/kg)	Power required for head				Power required for body (W/kg)	tMax (ms)	Relative head rotation
		Total (W/kg)	Inertia (W/kg)	Drag (W/kg)	Added Mass (W/kg)			
1	2210	1650	1280	104	264	564	3.1	0.21
2	2240	1510	1110	107	289	730	2.7	0.23
3	3410	2520	1750	265	504	884	2.4	0.35
4	3530	2440	1820	215	404	1090	2.5	0.35
5	2700	1700	1230	85.8	385	1000	2.4	0.25
6	2940	2200	1630	147	423	740	2.7	0.29
Mean	2840	2000	1470	154	378	835	2.6	0.28
SD	560	439	300	71.3	89.0	194	0.3	0.06
min	1090	754	522	34.9	176	144	2.0	0.15
max	5550	3640	2970	379	844	2680	4.0	0.42

Table S2: Summarized output from calculations of the maximum muscle mass specific power requirement for snipefish dorsal head rotation. Average variables were calculated for each of the 6 individual (individ.) fish in our study. We also report the mean and standard (SD) deviation across individuals. Minimum (min) and maximum (max) values are calculated across all 30 strikes to show the range in the entire dataset. tMax indicates the time between strike onset and the time of maximum power requirement. The peak instantaneous power requirement for head rotation during feeding includes the power required to rotate the head itself and the power used in body recoil. We also show the breakdown of the different contributions to the power requirement for head rotation: power to overcome inertial forces, power to overcome hydrodynamic drag, and power to overcome added mass of the surrounding water. We report the relative head rotation at time of peak power requirement as a proportion.